Journal of Alloys and Compounds 509 (2011) 9542–9548

Contents lists available at ScienceDirect

Journal of Alloys and Compounds

journal homepage: www.elsevier.com/locate/jallcom

A precursor route to synthesize mesoporous γ-MnO_2 microcrystals and their applications in lithium battery and water treatment

Jingfa Li, Baojuan Xi, Yongchun Zhu*, Qianwen Li, Yan Yan, Yitai Qian*

Department of Chemistry, Hefei National Laboratory for Physical Sciences at Microscale, University of Science and Technology of China, 96 Jinzhai Road, Hefei, Anhui 230026, PR China

ARTICLE INFO

Article history:
Received 26 May 2011
Received in revised form 19 July 2011
Accepted 20 July 2011
Available online 27 July 2011

Keywords:
Nanostructures
Chemical synthesis
Thermal analysis

ABSTRACT

$MnCO_3$ microstructures, including 2.3 μm microplates with the thickness of 200 nm and 3.1 μm microspheres stacked with 50 nm-thick sheets, were hydrothermally prepared in the assistance of sodium dodecyl benzene sulphonate (SDBS) and dodecyl sulfonic acid sodium (SDS), respectively. With the as-synthesized $MnCO_3$ as precursors followed by annealing at 400 °C for 4 h, mesoporous γ-MnO_2 microplates and microspheres with the pore size of 4–50 nm, which basically preserved the initial shapes, were obtained. The Brunauer–Emmett–Teller surface areas of the as-prepared γ-MnO_2 microplates and microspheres were 52.1 $m^2 g^{-1}$ and 50.2 $m^2 g^{-1}$, respectively. The electrochemical property tests over Li^+ batteries showed that the initial discharge capacity of γ-MnO_2 microplates and microspheres were 1997 mAh g^{-1} and 1533 mAh g^{-1}. Noticeably, even after 100 cycles, the discharge capacity of γ-MnO_2 microplates was still as high as 626 mAh g^{-1}, indicating the decent cycle behavior. In addition, mesoporous γ-MnO_2 was also applied as adsorbents in water treatment, and γ-MnO_2 microplates and microspheres could remove about 55% and 80% of Congo red.

1. Introduction

It is well known that manganese dioxide can form several kinds of polymorphs such as α-, β-, γ- and δ-type according to the different linkage patterns of basic unit [MnO_6] octahedral [1]. Among all the structures, γ-MnO_2, which is considered to be an intergrowth of ramsdellite (1 × 2 tunnels) and pyrolusite (1 × 1 tunnels) [2], has wide applications in lithium ion battery [3–5], electrochemical supercapacitors [6,7], dry-cell batteries [8,9], catalysts [10–14], and water-purifying agents [15]. Therefore, study of synthesis and application over γ-MnO_2 has attracted much more interest.

Recently, a variety of strategies have been developed and employed to fabricate γ-MnO_2 with well-defined morphologies because of the strong size- or structure-dependent properties. In general, these methods can be divided into two routes. One is direct growth of γ-MnO_2. For instance, electrolytic method [16–19], solid-state reaction [6], room temperature reduction [7], and hydrothermal method [20,21] have been adopted to synthesize γ-MnO_2 with various shapes. Recently, precursor-based routes followed by certain post-treatments have already been designed to obtain inorganic nanomaterials efficiently owing to the definite transformation to the aimed materials through the removal of organic ingredients [22–25]. It generally involves procedures of shape-controlled synthesis and subsequent process of the precursors treated at certain conditions to get γ-MnO_2 structure. For example, $MnCO_3$ solid microspheres and microcubes synthesized in hydrothermal condition were oxidized by $KMnO_4$ solution at room temperature, and then hollow microspheres and microcubes composed of γ-MnO_2 nanosheets were finally obtained [26]. Porous γ-MnO_2 hollow microspheres and hollow microcubes composed of particles have also been produced by calcining the $MnCO_3$ synthesized with ammonium hydrogen carbonate as the precipitant during hydrothermal courses [3].

Herein, we report a facile route to fabricate manganese carbonate ($MnCO_3$) structures with the shapes of microplates and microspheres just by changing the surfactants applied in the synthesis system. After annealing at 400 °C for 4 h in air, mesoporous γ-MnO_2 microcrystal with the pore size of 4–50 nm was obtained, which still maintained the initial morphologies. The electrochemical measurement results over Li^+ batteries indicated that the initial discharge and charge capacities of the as-prepared γ-MnO_2 microplates were 1997 mAh g^{-1} and 1271 mAh g^{-1}, respectively. And the discharge capacity of γ-MnO_2 microplates was still 626 mAh g^{-1} in the current density of 100 mA·g^{-1} even after

* Corresponding authors. Tel.: +86 551 3602942; fax: +86 551 3607402.
E-mail addresses: ychzhu@ustc.edu.cn (Y. Zhu), ytqian@ustc.edu.cn (Y. Qian).

0925-8388/$ – see front matter.
doi:10.1016/j.jallcom.2011.07.064

100 cycles, indicating its potential application in Li-ion batteries. The adsorptive experiments for Congo red also indicated the potential application as the water-purifying agents.

2. Experimental details

2.1. Synthesis of the manganese carbonates precursors and γ-MnO_2 samples

In a typical procedure, 3 mmol surfactant (SDBS or SDS) was dissolved in 45 mL of distilled water. Subsequently, 2 mmol $MnCl_2{\cdot}4H_2O$ was added to form a homogeneous solution under stirring and then 3 mmol urea was added into the above solution. After stirring continuously for 30 min, the solution was transferred into a Teflon-lined stainless-steel autoclave (capacity: 60 mL), sealed and heated at given temperatures for 12 h in an electronic oven. The autoclave was cooled naturally to room temperature. The precipitates were centrifuged and sequentially washed with water and ethanol repeatedly. The precursor of $MnCO_3$ was dried at 60 °C in a vacuum. Finally, porous γ-MnO_2 crystals were obtained by thermal treatment of the as-prepared $MnCO_3$ precursor at 400 °C for 4 h.

2.2. Structural characterization

The samples were characterized by X-ray diffraction (XRD, Philips X'Pert Pro Super diffractometer with CuKα radiation (λ = 1.54178 Å)); Field Emission Scanning Electronic Microscopy (FESEM, JSM-6700F); Transmission Electron Microscopy (TEM, HITACHI-H7650); High-Resolution Transmission Electron Microscopy (HRTEM, JEOL-2010, 200 kV); X-ray Photoelectronic Spectrum measurements (XPS) were performed by using a VGESCA-LABMKIIX-ray photoelectronic spectrometer. The TGA date was collected by a TGA-2050 (TA Corp.) themogravimeter; BET and Adsorption Analysis (Micrometrics ASAP 2020M).

2.3. Electrode fabrication and electrochemical characterization

The electrochemical measurements were carried out using CR 2032 coin cells with lithium metal as the counter and reference electrodes. The working electrodes consisted of mixing 85 wt% active materials (MnO_2), 10 wt% conductivity agent (Vulcan XC-72 carbon), and 5 wt% polyvinylidene fluoride (PVDF) with N-methylpyrrolidone (NMP) as the solvent and coated onto a copper foil substrate. The electrolyte was the solution of 1 M $LiPF_6$ in a mixture of ethylene carbonate (EC) and diethyl carbonate (DEC) with the volume ratio of 1:1. The electrodes were dried at 110 °C in a vacuum furnace for 12 h before use. The CR 2032 coin cells were assembled in a glove box under an argon atmosphere. For long-term cycling experiments, the cells were charged and discharged between 0.01 and 3.3 V (versus Li/Li^+) using a constant current density of 100 mA g^{-1}. The electrochemical properties of these electrodes were investigated using the Land battery measurement system (Wuhan, PR China) at room temperature.

2.4. Water treatment experiments

Commercial manganese dioxide powders were purchased from Shanghai Chemical Reagents Company and used without any treatment. The reaction was carried out in a 250 mL glass flask, which contained 70 mL Congo red solution (20 mg L^{-1}). The pH of the solution was neutral at about 7.2 without adjusting. The solution reacted at room temperature under continuously stirring, then 30 mg mesoporous γ-MnO_2 microspheres, microplates or commercial MnO_2 powders were added into the solution, respectively. The solution was centrifuged immediately for UV–vis absorption measurement in order to remove the adsorbent particles for preventing the particles to scatter the incident beam. The concentration of Congo red was monitored at its maximum absorption wavelength of 493 nm at different time intervals by colorimeter with a TU-1900 UV–vis spectrometer (Beijing).

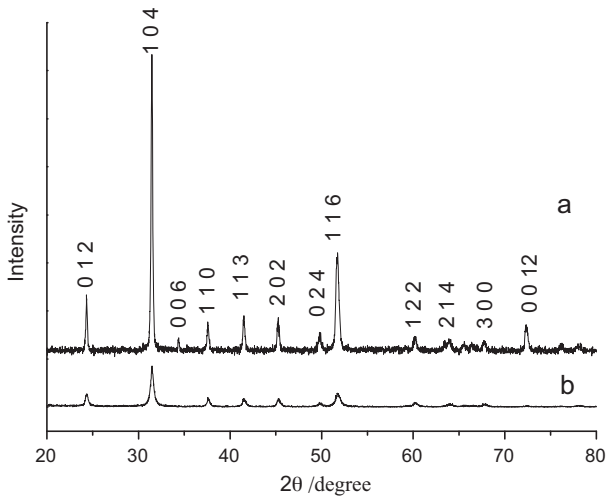

Fig. 1. XRD patterns of the precursor $MnCO_3$ prepared at 110 °C with different surfactants: (a) SDBS, (b) SDS.

3. Results and discussion

3.1. Preparation of the $MnCO_3$ precursors

The X-ray diffraction (XRD) patterns of the products prepared by using different surfactants are shown in Fig. 1a and b. All the diffraction peaks from Fig. 1a and b can be indexed to hexagonal phase of $MnCO_3$, which is consisted with the reported data (JCPDS Card 86-0172).

Fig. 2a shows panoramic FESEM images of $MnCO_3$ product prepared at 110 °C for 12 h by adding 3 mmol SDBS, which reveal

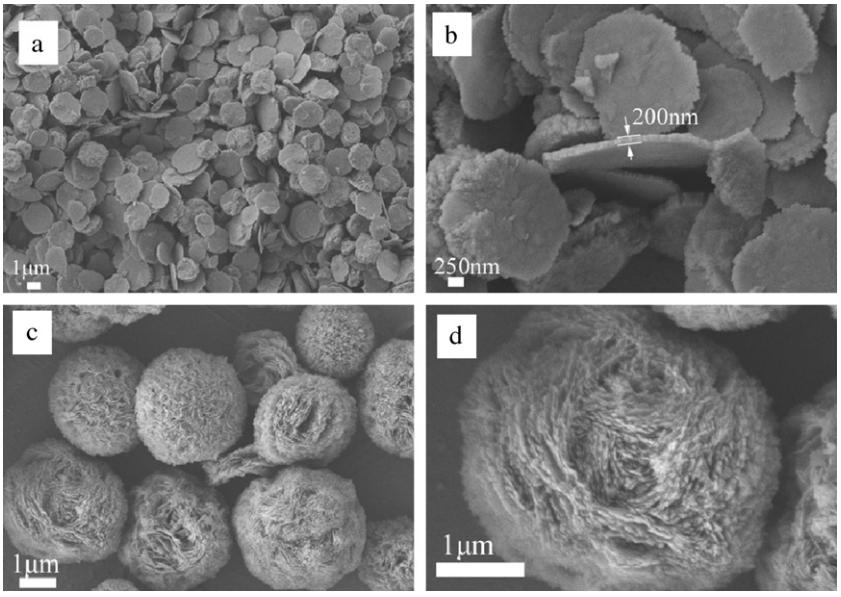

Fig. 2. Low and high magnification FESEM images of $MnCO_3$ prepared at 110 °C for 12 h in the presence of 3 mmol SDBS (a and b) or SDS (c and d).

the scaled-up synthesis of $MnCO_3$ microplates. From the high-magnification images of Fig. 2b, it can be observed that these microplates are uniform with the average diameter of 2.3 μm and thickness of about 200 nm. Further careful observation over these panels, the microplate's surfaces are rough. Series of experiments at different temperatures were also carried out (not shown here), and the results showed that the optimal temperature was 110 °C to produce the relatively uniform microplates shapes. The chemical reactions equations are shown as follows:

$$Mn^{2+} + SDBS \xrightarrow{stirred} Mn(DBS)_2 + 2Na^+$$

$$NH_2CONH_2 + 2H_2O \xrightarrow{heated} CO_3^{2-} + 2NH_4^+$$

$$Mn(DBS)_2 + CO_3^{2-} + 2Na^+ \xrightarrow{heated} MnCO_3 \downarrow + SDBS$$

Interestingly, relatively uniform microspheres with the average diameter of 3.1 μm stacked with thin sheet are obtained when SDBS is replaced by SDS at 110 °C. As shown in Fig. 2c and d, these microspheres are in a high yield and assembled by thin sheet with thickness of about 50 nm.

3.2. Preparation of mesoporous MnO_2 particles

Before calcining the precursors to obtain manganese dioxide, we carried out the thermogravimetric analysis (TGA) to guide us to adopt appropriate calcining temperature. The measurements were taken in the constant flow of dry air and the sample temperature was raised at a ramp rate of 10° min^{-1} to 800 °C. As shown in Fig. 3, three major stages of weight loss can be observed. The first weight drop (ca. 1.47%) is before 350 °C due to desorption of the physically and chemically absorbed water. The second drop occurs between 365 °C and 489 °C (ca. 25.4%), which is caused by the transformation from $MnCO_3$ to MnO_2. The third loss (ca. 3.98%) happening between 490 °C and 564 °C, corresponds to the transition from MnO_2 to Mn_2O_3, which is in well agreement with the previous report [3].

On the basis of the TGA results, we chose 400 °C as the calcining temperature in order to obtain pure MnO_2 phase. Fig. 4a and d shows the XRD patterns of the products after calcinations of $MnCO_3$ microplates or microspheres, which are consistent with the previous reports [3,27], indicating the as-calcined products were γ-MnO_2. Fig. 4b and c shows the typical images of γ-MnO_2 which were calcined from $MnCO_3$ microplates prepared using SDBS as surfactant. It is obvious that the final sample reserved the overall morphologies of the precursor after calcining. However, the surfaces of the plates are full of pores from the results of high-magnification FESEM (Fig. 4c). Fig. 4e and f indicates that the calcined products also kept the shape of $MnCO_3$ microsphere.

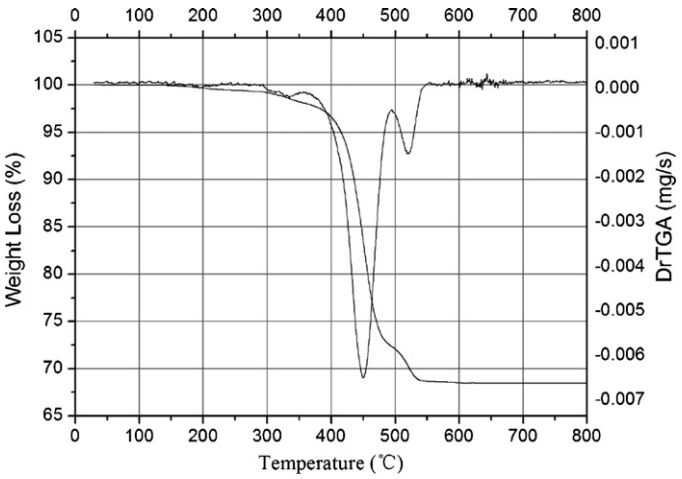

Fig. 3. TGA and DrTGA curve of the $MnCO_3$ microcrystal prepared at 110 °C using SDBS as surfactant.

Fig. 5a and c shows the TEM images of a single γ-MnO_2 microplate and a microsphere, respectively. Fig. 5b and d is detailed observation obtained from the microplate and component sheet surfaces marked in Fig. 5a and c, displaying the porous configuration (shown by the arrows) generated by the transformation of $MnCO_3$ into MnO_2 in the calcining process.

To assess the chemical composition of these samples, energy dispersive spectrometry (EDS) analysis and XPS measurement are employed together. As shown in Fig. 5e, the results confirm the presence of Mn and O elements and the atom mole rate is close to 1:2. The C and Cu elements should be from the copper grid. In Fig. 6, the binding energies are corrected for specimen charging by referencing the C 1s to 284.60 eV. The survey spectrum (Fig. 6a) indicates the presence of Mn and O as well as C from the reference and the absence of impurity such as Na^+. The high-resolution spectrum of Mn $2p_{3/2}$ and $2p_{1/2}$ are found to be 642.2 eV and 654.1 eV, respectively. The results agree well with those reported data for MnO_2 [28], indicating that the oxidation state of manganese is +4. In addition, the atom molar rate is 1:1.91, which confirms its

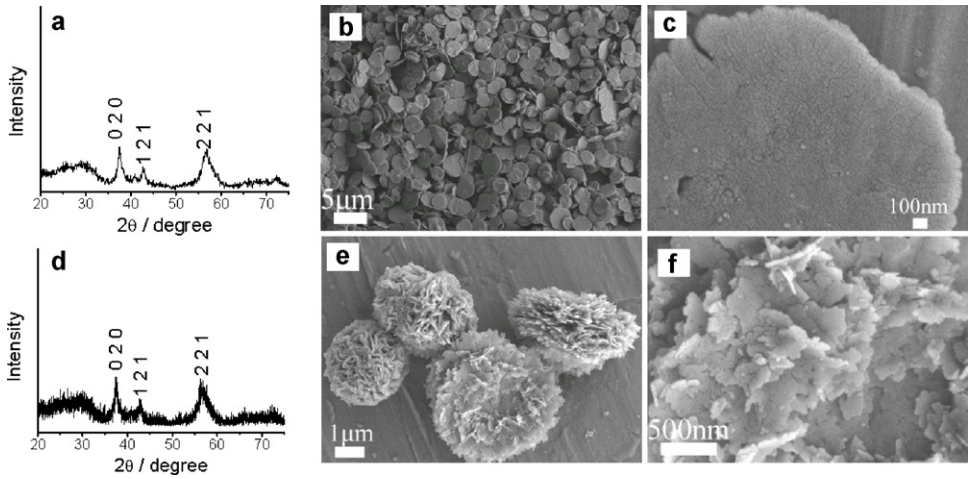

Fig. 4. The corresponding XRD patterns of the as-calcined product with porous microplate (a) and microsphere (d) shapes. Low and high magnification SEM images of the porous MnO_2 (b and c) microplates and (e and f) microspheres composed of thin sheet calcined from $MnCO_3$ particles prepared with SDBS and SDS as surfactant at 110 °C, respectively.

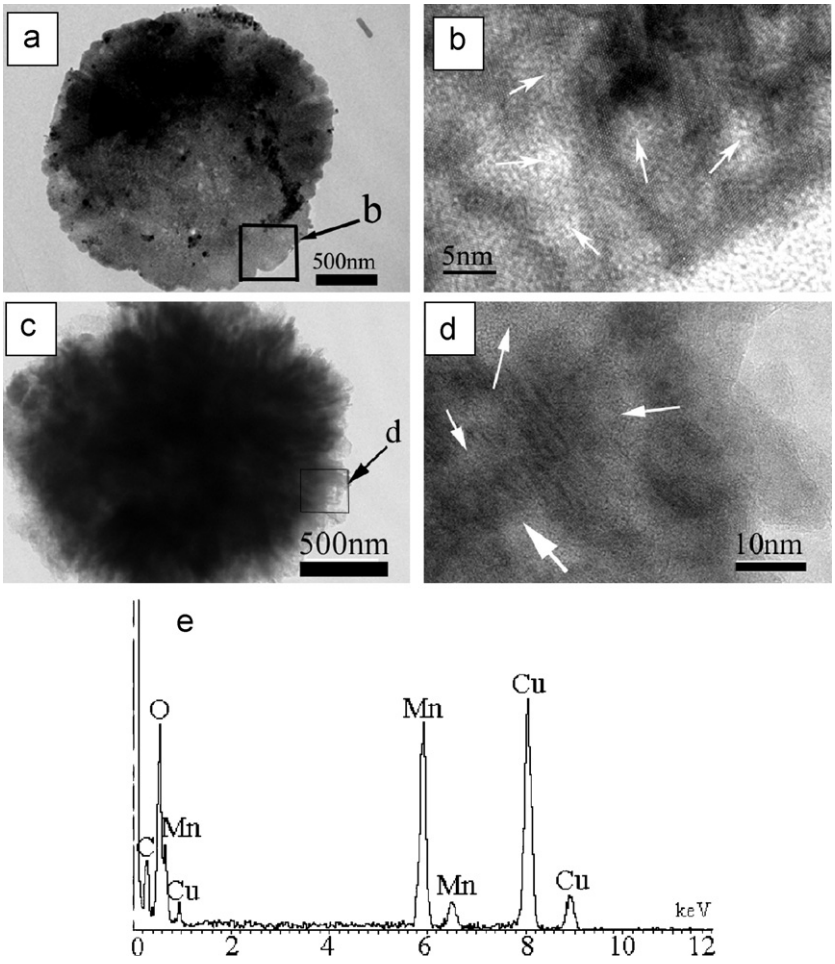

Fig. 5. (a–e) TEM and HRTEM images of the as-calcined product of γ-MnO_2 with porous microplate shapes (a and b) and microspheres composed of thin sheet (c and d). (e) EDS pattern of the porous γ-MnO_2 microcrystal.

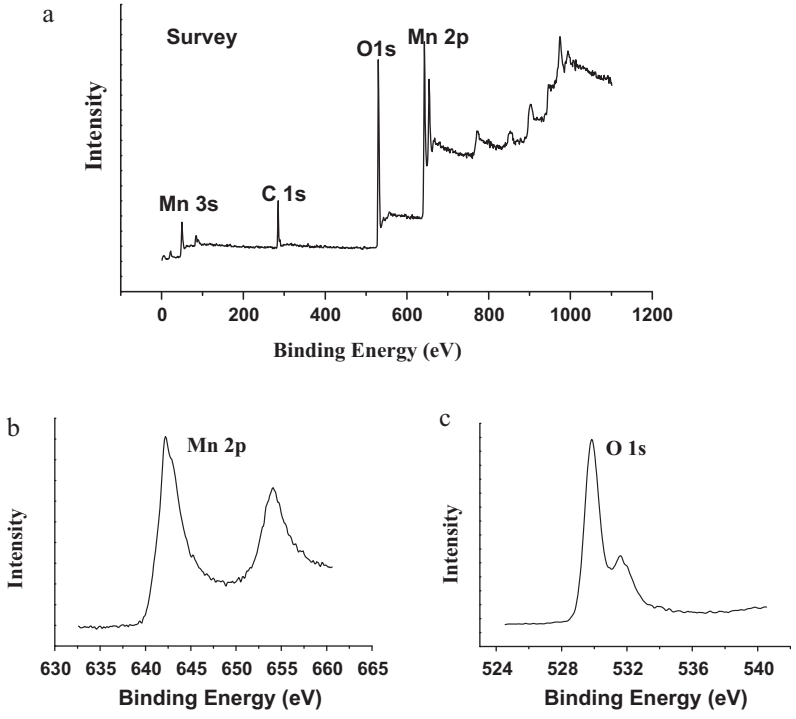

Fig. 6. Typical XPS spectra for MnO_2 microplates prepared by calcinations at 400 °C for 4 h.

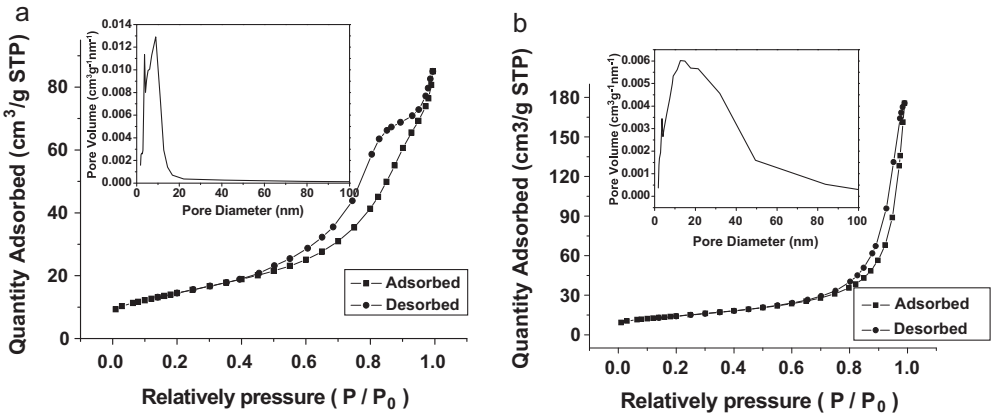

Fig. 7. N_2 adsorption/desorption isotherms and BJH pore size distribution plots (inset) of porous γ-MnO_2 microplates (a) and microspheres composed of thin sheet (b).

stoichiometric proportion and corresponds to EDS analysis. Thus, based on all the results mentioned above, it is clear that the composition of the crystallites calcined from the precursor is manganese dioxide.

3.3. BET and adsorption analysis

To evaluate the surface areas of the γ-MnO_2 microplates and microspheres composed of thin sheets and determine the pore structures of the samples, N_2 adsorption/desorption isotherms were investigated. Fig. 7 shows the N_2 adsorption/desorption isotherms and the Barrett–Joyner–Halenda (BJH) pore size distribution curves (inset) of γ-MnO_2 microplates and microspheres from N_2 desorption isotherms. The measurements showed that the BET surface area of porous microplates was 52.1 $m^2\,g^{-1}$ and the pore size distributions were centered at 3.6 and 8.9 nm according to the BJH method. Moreover, the BET surface area of microspheres was estimated to be 50.2 $m^2\,g^{-1}$, and there were two small pore distribution peaks at 3.6 nm and 12.6 nm. Both of the isotherms are identified as type IV, determining γ-MnO_2 structures to be mesoporous [29]. The distribution of the pore diameter of the microplates and microspheres is arranged by 3.6–15 nm and 3.6–80 nm

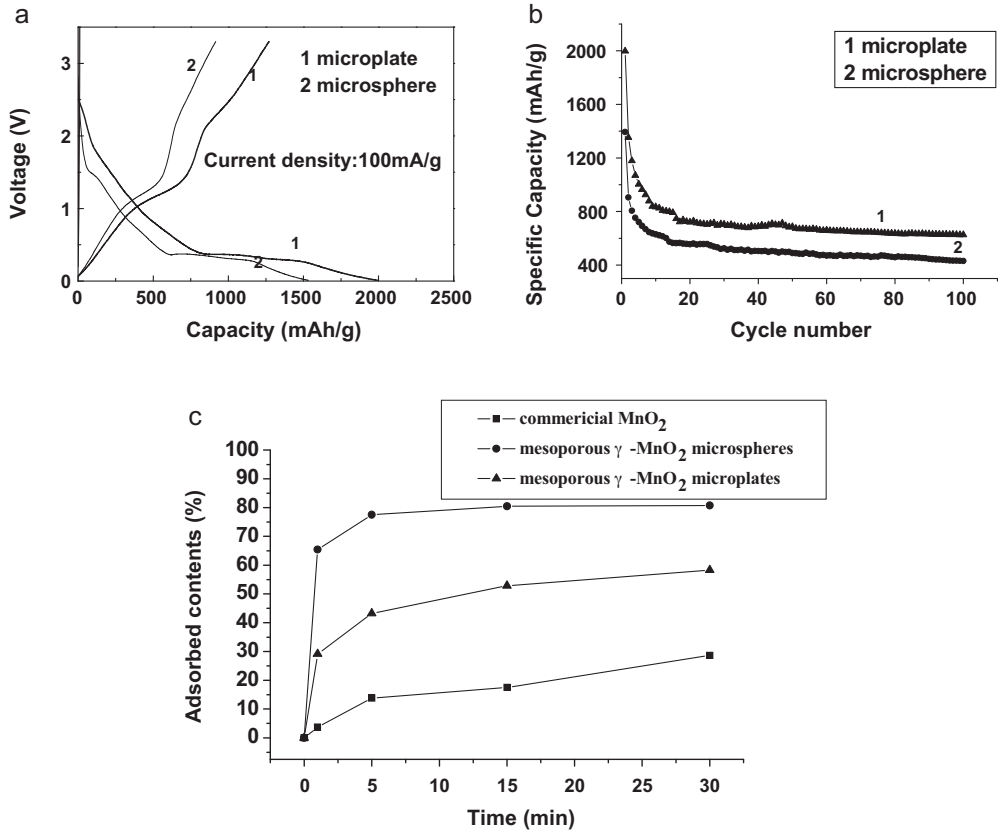

Fig. 8. (a) First discharge–charge curves and (b) cycle performances of γ-MnO_2 microplates (1) and microspheres (2) between 0.01 and 3.3 V vs Li/Li^+ at a constant current density of 100 mA g^{-1}. (c) Curves of adsorbed contents of Congo red solutions with different time over the as-prepared porous γ-MnO_2 microplates, microspheres, and commercial MnO_2 powders.

respectively, which may affect the capacity of the sample in Li-ion battery.

3.4. Application of the as-prepared samples in lithium batteries

It has been reported that the nanostructed 3d transition-metal oxides such as nickel oxides, cobalt oxides and iron oxides exhibit reversible capacities about three times larger than graphite [30]. Some researches have also shown that porous structure is an ideal host for reversible Li^+ intercalation with a high stability [31], which can buffer the volume expansion and shorten the diffusion paths of lithium ions. Hence, electrochemical performance of the as-prepared MnO_2 nanostructures was evaluated in the cell configuration of Li/MnO_2. Fig. 8a shows the charge/discharge curves of γ-MnO_2 microplates (1) and microspheres (2). From Fig. 8a, during the discharge process, a plateau can be found at about 0.4 V for both samples, and the initial discharge capacities of γ-MnO_2 microplates are 1997 mAh g^{-1} at the current density of 100 mA g^{-1} in the potential window of 0.01–3.3 V, larger than that of microspheres (1553 mAh g^{-1}). That may be attributed to the narrow distribution of the pore diameter of the microplates, which offers the short Li^+ ion diffusion lengths, high surface contact with electrolyte (high surface area), and the extra active position (surface pores). The higher first discharge capacities (theoretical capacity for MnO_2 was 1233 mA g^{-1}) may be due to the formation of solid electrolyte interface (SEI) layer and a polymer/gel-like film [32], and this similar phenomena was also observed about other transition-metal oxides (such as CoO, Fe_2O_3, NiO, etc.) [32–34]. However, in the following charge process the lithium extraction shows a large irreversibility, the first charge capacities of microplates and microspheres were 1271 mAh g^{-1} and 916 mAh g^{-1}, and the charge retentions were 63.7% and 59.0%, respectively, and the irreversible capacity is approximately 700 mAh g^{-1}. This large capacity loss is attributed to some possible irreversible processes, such as decomposition of electrolyte to form a protective film on the surface of manganese oxides electrode surface [34].

The cyclical stabilities of the as-prepared γ-MnO_2 samples were also tested. Fig. 8b shows that the capacity tends to level off after 15 cycles, while that of the first few cycles degrades steeply. The possible cause to the capacity decreasing so deeply during the first few cycles is the formation of the passive SEI film, or decomposition of electrolyte to form a protective film on the electrode surface [35]. Specifically, although the capacity still decays gradually over cycling, the capacities of γ-MnO_2 microplates and microspheres are 626 mAh g^{-1} and 431 mAh g^{-1} after 100 cycles, respectively, which is still about 68.3% and 15.9% higher than the theoretical capacity of graphite (372 mAh g^{-1}) [30]. Based on all the above results, it is evident that the mesoporous microplate is a better candidate than microsphere with the higher lithium storage capacity, lower irreversible loss, and excellent cycling performance.

3.5. Adsorption measurements of organic dyes of the porous γ-MnO_2 microplates and microspheres

As-prepared porous γ-MnO_2 microstructures were also investigated as effective water-purifying agents. For comparison, an experiment with commercial MnO_2 was also performed under the same conditions. The characteristic adsorption of Congo red at 493 nm was chosen for monitoring the adsorption process. Fig. 8c shows the curves of adsorbed contents of Congo red solution with different time over the as-prepared porous γ-MnO_2 microplates, microspheres and commercial MnO_2 powders. It is obvious that porous γ-MnO_2 microplates and microspheres are more effective than commercial MnO_2 powders to remove Congo red from water. The adsorption process is rapid in the early stage, with an absorbance of about 65% after a reaction time of only 1 min for γ-MnO_2 microspheres. After 30 min stirring continuously, the adsorbance is close to 80% for microspheres, 55% for microplates and 25% for commercial powders, respectively. The contrast of the adsorbance between the microplate and microsphere samples is owing to the latter assembled nanosheet as building blocks possessing the higher average pore diameter and supplying more interlayer spaces, which ensures Congo red species entered and interacted with the surface of porous γ-MnO_2 structure. The mechanism for the adsorption was proposed to be the electrostatic attraction between the surface of porous γ-MnO_2 structure and the Congo red species in solution at pH 7.2 [36].

4. Conclusions

In summary, mesoporous γ-MnO_2 microcrystal with the pore size of 4–50 nm were obtained by a precursor-based route without obvious change of the morphologies after calcinations. The electrochemical measurement results over Li^+ batteries indicated that the initial discharge and charge capacities of the as-prepared γ-MnO_2 microplates were 1997 mAh g^{-1} and 1271 mAh g^{-1}, respectively, and the discharge capacity was still 626 mAh g^{-1} even after 100 cycles. In addition, the adsorptive experiments for Congo red show that porous γ-MnO_2 microspheres have an effective adsorbance reaching 80% after stirring for 30 min. Both the results indicate the potential application in Li battery and water treatment.

Acknowledgements

The authors thank Prof. J. Chen et al. (Nankai University) for their help with the electrochemical experiments and results discussion. The financial supports of this work, by the 973 Project of China (No. 2011CB935900) and the National Nature Science Fund of China (No. 91022033), are gratefully acknowledged.

References

[1] Z.Q. Li, Y. Ding, Y.J. Xiong, Q. Yang, Y. Xie, Chem. Commun. 91 (2005) 8–920.
[2] F.Y. Cheng, J.Z. Zhao, W.N. Song, C.S. Li, H. Ma, J. Chen, P.W. Shen, Inorg. Chem. 45 (2006) 2038.
[3] J.Z. Zhao, Z.L. Tao, J. Liang, J. Chen, Cryst. Growth Des. 8 (2008) 2799.
[4] M. Minakshi, M. Blackford, M. Ionescu, J. Alloys Compd. 509 (2011) 5974.
[5] S. Jouanneau, S. Sarciaux, A. Le Gal La Salle, D. Guyomard, Solid State Ionics 40 (2001) 223–232.
[6] D.L. Fang, B.C. Wu, A.Q. Mao, Y. Yong, C.H. Zheng, J. Alloys Compd. 507 (2010) 526.
[7] D.L. Fang, B.C. Wu, A.Q. Mao, Y. Yan, C.H. Zheng, J. Alloys Compd. 505 (2010) 555.
[8] M. Thackeray, Prog. Solid State Chem. 25 (1997) 1–71.
[9] G.Q. Zhang, X.G. Zhang, Solid State Ionics 160 (2003) 155–159.
[10] M. Ahn, T.R. Fillry, C.T. Jafvert, L. Nies, L. Hua, J. Cruz, Environ. Sci. Technol. 40 (2006) 215.
[11] K.A. Barrett, M.B. Mcbride, Environ. Sci. Technol. 39 (2005) 9223.
[12] Y. Sekine, Atmos. Environ. 36 (2002) 5543.
[13] M. Baldi, E. Finocchio, C. Pistarino, G. Busca, Appl. Catal. A 173 (1998) 61.
[14] M. Te, H.C. Foley, Appl. Catal. A 119 (1994) 97.
[15] J. Post, Proc. Natl. Acad. Sci. U.S.A. 96 (1999) 3447.
[16] G.J. Moore, R. Portal, A. Le Gal La Salle, D. Guyomard, J. Power Sources 97–98 (2001) 393.
[17] M. Ghaemi, Z. Biglari, L. Binder, J. Power Sources 102 (2001) 29–34.
[18] M.S. Wu, J.T. Lee, Y.Y. Wang, C.C. Wan, J. Phys. Chem. B 108 (2004) 16331.
[19] W. Scott, D. Frank, H. Feddrix, S. Marion, T. Norby, Solid State Ionics 152–153 (2002) 695.
[20] F. Teng, S. Santhanagopalana, Y. Wang, D.D. Meng, J. Alloys Compd. 499 (2010) 259.
[21] C.Z. Wu, W. Xie, M. Zhang, J.L. Yang, Y. Xie, Chem. Eur. J. 15 (2009) 492.
[22] S. Farhadi, N. Rashidi, J. Alloys Compd. 503 (2010) 439.
[23] M. Popa, J.C. Moreno, J. Alloys Compd. 509 (2011) 4108.
[24] H. Zhang, Y.J. Chen, J.H. Ma, H.X. Tong, J. Yang, D.W. Ni, H.M. Hu, F.Q. Zheng, J. Alloys Compd. 509 (2011) 6616.
[25] F. Li, J.F. Wu, Q.H. Qin, Z. Li, X.T. Huang, J. Alloys Compd. 492 (2010) 339.
[26] J.B. Fei, Y. Cui, X.H. Yan, W. Qi, Y. Yang, J.B. Li, Adv. Mater. 20 (2008) 452.
[27] J.K. Yuan, K. Laubernds, Q.H. Zhang, S.L. Suib, J. Am. Chem. Soc. 125 (2003) 4966.
[28] V. Subramanian, H.W. Zhu, B.Q. Wei, J. Phys. Chem. B 109 (2005) 20207.
[29] A. Vinu, D.P. Sawant, K. Ariga, M. Hartmann, S.B. Halligudi, Microporous Mesoporous Mater. 80 (2005) 195.

[30] M. Winter, J.O. Besenhard, M.E. Spahr, P. Novak, Adv. Mater. 10 (1998) 725.
[31] I. Moriguchi, R. Hidaka, H. Yamada, T. Kudo, H. Murakami, N. Nakashima, Adv. Mater. 18 (2006) 69.
[32] S. Laruelle, S. Grugeon, P. Poizot, M. Dolle, L. Dupont, J.M. Tarasconz, J. Electrochem. Soc. 149 (2005) A627.
[33] J. Chen, L.N. Xu, W.Y. Li, X.L. Gou, Adv. Mater. 17 (2005) 582.
[34] J.M. Tarascon, M. Armand, Nature 414 (2001) 359.
[35] M.S. Wu, P.C. Chiang, J. Electrochem. Commun. 8 (2006) 383.
[36] L.S. Zhong, J.S. Hu, H.P. Liang, A.M. Cao, W.G. Song, L.J. Wan, Adv. Mater. 18 (2006) 2426.